NASA/CR-96- 207820

IN-11-CR
114 6x 7

Final Report on NASA Grant NAG-4988

Temporal Evolution of SL-9 Impact Sites on Jupiter and Global Maps of Jupiter from Multi-Observatory Visible and Infrared Images

Period: 1/1/96-12/31/96

Sanjay S. Limaye

Space Science & Engineering Center

University of Wisconsin-Madison
1225 West Dayton Street
Madison, WI 53706-1695

Summary

The objective of this research was to investigate the temporal behavior of the impact features on Jupiter created by the fragments of the Shoemaker Levy -9 comet that collided with the planet in July 1994. The primary observations used in the study were ground based images of Jupiter acquired from the Swedish Solar Vacuum Tube on the island of La Palma in the Canary Islands. The measurement of position of the impact features in images acquired immediately after the impact over a period of a few days revealed that the apparent drift rates were too high and that a repetitive pattern could be seen in the longitude position on successive rotations. This could be explained only by the fact that the measured longitudes of the impact sites were being affected by parallax due to a significant elevation of the impact debris above the nominal cloud top altitude value used for image navigation. Once the apparent positions are analyzed as a function of the meridian angle, the parallax equation can be used to infer the height of the impact features above the cloud deck, once the true impact position (longitude) for the feature is known. Due to their inherent high spatial resolution, the HST measurements of the impact site locations have been accepted widely. However, these suffer from the parallax themselves since few of them were obtained at central meridian. Ground based imaging have the potential to improve this knowledge as they do observe most of the impact sites on either side of the central meridian, except for the degraded resolution. Measurements over a large number of images enables us to minimize the position error through regression and thus estimate both the actual impact site location devoid of parallax bias, and also of the altitude level of the impact debris above the cloud deck. With rapid imaging there is the potential to examine the time evolution of the altitude level. However, this aspect could not be pursued under the limited resources available under this grant.

Several hundred ground based images were processed, navigated and subjected to the impact site location measurements. HST images were also acquired and used to calibrate the results and to improve the sample. The resources available enabled an in-depth study only of impact site A, however, many more images have since become available through the global network observations through Lowell Observatory.

Preliminary results were presented at the International Conference on SL-9 and Jupiter, Paris France in July 1996. A paper based on the work was prepared. Its submission for publication has been delayed pending completion of the HST observations based upon some critical comments made by colleagues and potential reviewers. A copy of the manuscript as it currently exists is attached to this report.

Parallax determination from position measurements of Fragment A

The relationship between the measured parallax in longitude and the altitude of a feature above a reference surface of Jupiter is shown in the figure below. The latitude is assumed to be representative of the impact features for the SL -9 fragments (45°, planetocentric).

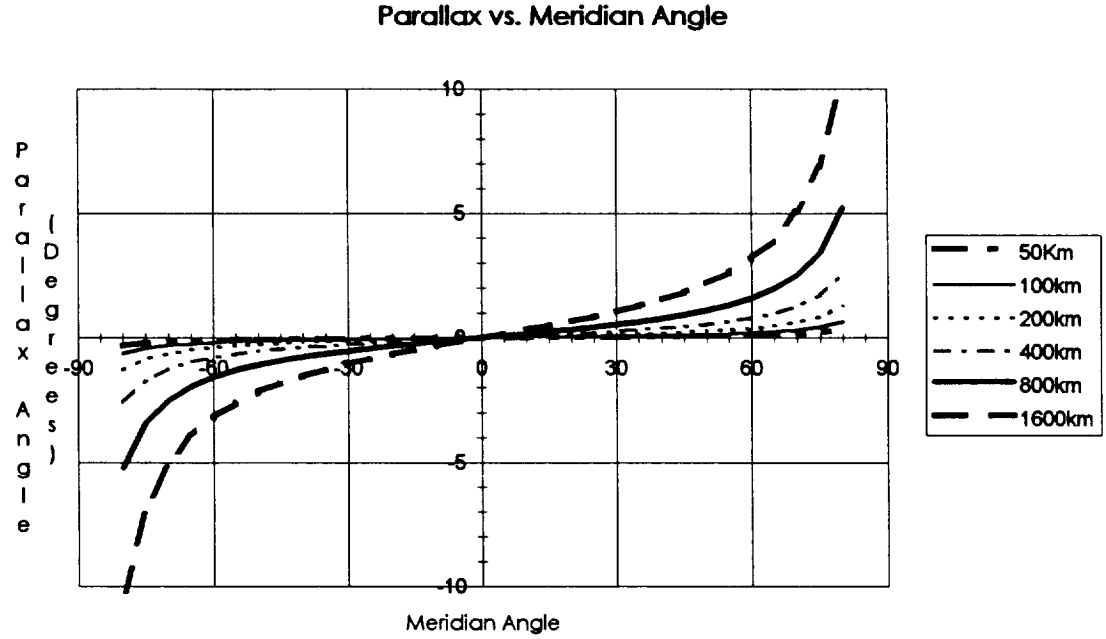

Figure 1. Longitude parallax angle in degrees vs. position angle from the central meridian for a given feature altitude in km. The characteristic shape for the family of curves evident at high meridian angles is evident in the actual measurements. Figure 2 below provides a finer view.

It is apparent that measuring the apparent location of the feature as far away from the central meridian as possible is preferred, particularly for low resolution images and for ground based observations that suffer from atmospheric seeing limitations. In practice, it is rarely possible to measure the locations of the features at very high meridian angles due to illumination (for images acquired by reflected sunlight). It is also apparent that the parallax effect should also affect the latitude measurements somewhat, although the magnitude is less pronounced. It should be noted that any error in the image navigation, particularly in the orientation becomes very obvious in the measured latitude of the feature as the planet rotates (assuming that the actual movement of the feature in the north-south direction is negligible).

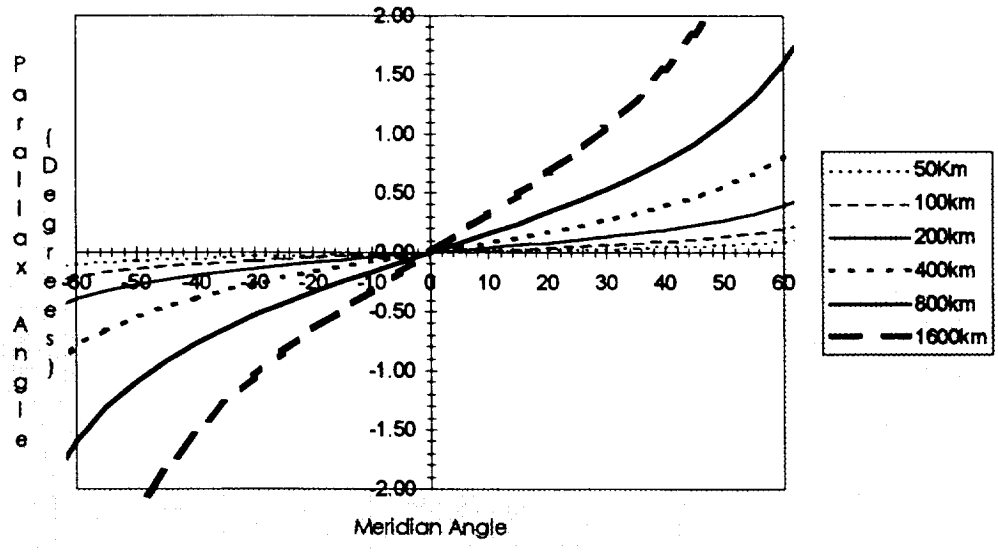

Figure 2. Longitude parallax angle in degrees vs. position angle from the central meridian for a given feature altitude in km. For small separation of the feature from the central meridian, the parallax angle has an almost linear relationship with the meridian angle. The characteristic shape for the family of curves evident at high meridian angles is evident in the actual measurements.

The measurements for feature A made in images acquired at the Swedish solar telescope are given below. The results indicate that when parallax measurements for median angles > 30° are considered, the estimated altitude of the impact feature is 1242.4 ± 495 if the true longitude of Feature A is taken to be that given by the HST measurements (Hammel et al., 1995). The average latitude of the darkest core of the impact site from these measurements for the feature (taken to be the darkest location) is 45.52°S ± 0.6°. This is somewhat different from the impact latitude given by Hammel et al. (1995) for impact site A, -43.54° S ± 1.0 . A non-linear regression for both the altitude level and the true longitude of feature A yields the altitude to be 1645 km, and the System III longitude to be 186.34° ± 0.6 , which improves upon the Hammel et al. report of 186.3° ± 2.0.

References

Hammel H.B., R.F. Beebe, A.P. Ingersoll, G.S. Orton, J.R. Mills, A.A. Simon, P. Chodas, J.T. Clarke, E. De Jong, T.E. Dowling, J. Harrington, L.F. Huber, E. Karkoschka, C.M. Santori, A. Toigo, D. Yeomans, and R.A. West, 1995. HST imaging of atmospheric phenomenon created by the impact of comet Shoemaker-Levy 9, Science, 267, 1288-1296.

Pre-print of a paper being prepared for submission pending completion analysis of Hubble Space Telescope Images.

Vertical Level of Shoemaker Levy 9 Impact Sites on Jupiter from Visible Images Acquired from the Swedish Solar Telescope at La Palma

Sanjay S. Limaye
Space Science and Engineering Center
University of Wisconsin-Madison
1225 West Dayton Street
Madison, WI 53706

and

Mats Lindgren
Uppsala Astronomical Observatory
Box 515,
751 20 Uppsala, Sweden

xx Pages
3 Figures

December, 1996

To be Submitted to *Nature*

Abstract

Compelling evidence for a significant elevation of the level of the Shoemaker Levy 9 impact features above the Jovian cloud deck is provided by measurements of the apparent longitudinal drift on consecutive sightings of the same feature on different nights. When mapped into a latitude-longitude maps with the known figure of Jupiter at the level of the cloud-tops, these images reveal a significant spurious foreshortening of the impact sites as a function of separation from the central meridian. Longitudinal positions of the impact sites also reveal an apparent consistent drift between 1 to 2 degrees per hour on consecutive sightings of the same feature on different nights but the feature tracing essentially the same longitude range on these occasions. The most plausible explanation is due to parallax not compensated during the mapping or measurement process such that near the morning terminator the measured longitudes are more westward than the true longitude of the feature, and more easterly near the afternoon terminator. These observations are persuasive evidence of a significant vertical separation of the impact features above the cloud cover of Jupiter. Results indicate an altitude of about xxx km $\pm$ 200 km for site A and about 800 $\pm$ 300 km for site H for 2-5 hours after the impacts.

The impact of Comet Shoemaker-Levy 9 fragments onto Jupiter was observed by many telescopes around the world and from spacecraft. Several modeling efforts before and after the impact provided clues about the impact process and some information about how high the impact debris might reach above Jupiter's cloud tops. Much of this modeling was restricted to an short interval after the impact itself. Indications of the debris cloud that persisted in the atmosphere for a longer period is just becoming evident from the observations acquired in the days during and following the multiple impact events. Many of the Shoemaker Levy 9 comet fragment impact sites on Jupiter can be monitored from morning terminator to the afternoon terminator as the planet turns. These broadband visible light images acquired from the Solar Telescope of the Royal Academy of Sciences at La Palma (1) allow the features to be monitored for more than four hours between July 16-21, 1994 with approximately one minute time resolution. Spatial resolution of the images is between 0.3 - 1.5 arc seconds for much of the data (2).

The first clue to the high apparent altitude level of the cloud features were obtained when the images were mapped with a view to construct space-time composite global maps. During the nearly 4.5 hour observing period achieved each night, Jupiter rotates through nearly 160 degrees of longitude. Thus nearly half of the planet is viewed each night. Rapid imaging during this time period enabled monitoring the impact sites as the planet turned. The combination of impact times for several Shoemaker Levy 9 fragments and the observing period from La Palma resulted in many features being picked up near the morning terminator as soon as they came into view, and followed as they disappeared nearly 3 hours later over the evening terminator. Figure 1 shows three views of impact features corresponding to fragments A: near the morning terminator, close to the central meridian, and nearer the evening terminator. The left column shows the telescope view and the right column shows a rectilinear latitude-longitude map view (0.2

degrees/pixel). The mapping was done for the known figure of Jupiter at the cloud level (equatorial radius of 71,492 km, polar radius of 66,854 km). A significant change in the shape of the features is evident in the map projected images. The impact features appear severely foreshortened in map projected images such that the distortion is dependent on the separation from the central meridian, This distortion makes the feature appear further westward when near the morning terminator and more eastward when near the evening terminator. This occurs because the mapping process assumes a fixed radii oblate planet model for Jupiter, causing feature to be mapped at a different longitude when not on central meridian. The offset between the 'true' longitude and measured or apparent longitude indicates that the features must be much higher than the cloud deck. Note that the other prominent features on Jupiter, e.g. the Great Red Spot (GRS) and the white ovals do not suffer the same distortions. The direction of the distortion of the dark impact features is along the southwest-northeast direction near the morning terminator and in the northwest-southeast direction when the features are closer to the evening terminator. Such a shape distortion is consistent with the vertical level of the impact features much higher than that of the visible cloud deck.

Another clue to the higher vertical level of the features being higher than that of the cloud deck is provided by the apparent position of the impact features. Typically, the measured longitudes are more westward nearer the morning terminator and more eastward nearer the afternoon terminator as compared to the longitude of the features when observed at central meridian. Because of the spatial resolution of the images and small variations caused by atmospheric seeing (turbulence, presence of aerosols) in ground based images, longitude measurements in single images can be uncertain by as much as 0.2-0.4 degree in latitude or longitude (3). Figure 2 shows the latitude and longitude positions of impact features A and H measured over a four hour period on their first appearance on the Jovian disk as viewed from La Palma. The longitude corresponds to the position of the darkest point in the central core of the impact sites. The time is noted on the lower x-axis, while the difference between the longitude and the central longitude of Jupiter at the time of measurement is indicated on the upper x-axis scale. Despite the scatter in the position measurements caused mostly due to atmospheric seeing and perhaps due to small changes in the features themselves, a consistent and apparently linear trend is seen in the longitude measurements, whereas the latitude is comparatively constant. A linear regression fit for the apparent longitude drift of the features yields values of 1.5 and 2 degrees per hour. Such a drift is nearly two orders of magnitude greater than the - 5 to + 5 ms^{-1} speeds at the cloud level from Voyager data (Limaye, 1986) between -43° and - 45° latitude (4). The implied altitude difference of the impact features is also inconsistent with the infrared measurements indicate that the zonal flow decreases with height above the cloud deck by Gierasch et al., 1986 (5).

The magnitude of the apparent longitude drift is suggests that the measured longitudes do not correspond to the actual longitudes. This is further confirmed by the results of the drift rates measured for the same features on their next visibility period from La Palma. Due to the diffuse nature of the features, the darkest point within the impact site is taken as the 'core' of and tracked in consecutive images. Figure 3 shows the

darkness of the H impact feature as indicated by the darkest brightness (after the limb darkening is removed) on the first and third nights after the impact (July 18th and 21st, 1994). For 1 to 3 hours after the impact the feature is seen to get darker, with two reversals of the trend nearing the end of the observations. The initial darkening has also been observed at ultraviolet wavelengths from the Hubble Space Telescope observations (6). The two brightenings and dimmings may be indicative of the bouncing back of the debris material after the intial injection into the upper atmosphere that has been surmised from modeling (Mac Low, 1995; Mac Low and Zahnle, 1994). Other approaches to 'locating' a feature, e.g. the center of the dark area, etc. may lead to similar, perhaps improved results on the altitude estimates. Much of the error arises due to atmospheric seeing effects and limited resolution of the images. The magnitude and direction of the drift in longitude is same as before. However, the features are measured through the *same* apparent longitude region! For this to have occurred, the features would have had to drift more than 50 degrees in longitude eastwards since the first sighting and then reversed the direction of motion and raced back to nearly the same longitude position two nights later. The longitudinal drift of an impact feature on a given night (about 4.5 hours) is about 1-2 degrees/hour. However, the same features appears to retrace its path when seen again (two nights later from the same telescope). This implies an unphysical oscillatory motion, and can only indicate that the drift is spurious due to the uncompensated parallax caused by the vertical level difference between the features and the cloud deck in the mapping process. This is additional proof that the measured longitudes are affected by the altitude of the features.

This is illustrated in Figure 3 The circle represents the cross section of Jupiter at the latitude of the impact sites as viewed. The longitude in System III increases to the left of the central meridian and decreases to the right (eastward) in this figure. The image navigation and mapping process measures the *projected* location of the impact sites (at an altitude *above* the cloud deck) that results in an *apparent* longitude that is further westward than the true longitude of the impact feature (i.e. when the feature is measured to be at the central meridian), and further eastwards when the feature is to the east (right) of the central meridian. This is exactly what is observed. From the geometry, it is possible to compute the altitude level of the impact features knowing the parallax (the difference between the measured and actual longitudes of the feature), the angular separation from the central meridian, and the radius of Jupiter at the impact site latitude as:

$$h = R_\phi \, \mathrm{Cos}(\phi) \{ \mathrm{Sin}(\lambda_P) * \tan(\pi/2 - \alpha) \; - (1 - \mathrm{Cos}\lambda_P) \},$$

where, λ_P is the parallax angle, i.e. the difference between the apparent longitude λ_o of the feature and the actual longitude λ_F, α is the difference between the longitude of the feature ($=\lambda_{CM} - \lambda_F$)and the central meridian longitude λ_{CM}, ϕ is the planetocentric latitude of the feature, and R_ϕ is the radius of Jupiter at that latitude to the cloud top level.

The observed parallax in longitude is larger for greater separation of the feature from the central longitude as expected.

the error in h can be estimated from:

$$\delta h = R_\phi \cos(\phi) \{ \delta(\sin(\lambda_P)) * \tan(\pi/2 - \alpha) + \sin(\lambda_P)\, \delta(\tan(\pi/2 - \alpha)) - \delta(1 - \cos\lambda_P) \}$$
$$= R_\phi \cos(\phi) \{ \tan(\pi/2 - \alpha) \cos(\lambda_P)\, \delta\lambda_P + \sin(\lambda_P) \sec^2(\pi/2 - \alpha)\, \delta\lambda_F + \sin\lambda_P \delta\lambda_P \}$$

The "true" position of the impact feature (core) is taken from the table provided by Hammel et al. (7), and has an uncertainty of $\pm$ 2° in longitude ($\delta\lambda_P$). The uncertainty in the feature parallax is dominated by atmospheric seeing and is at least 0.2°, corresponding to one pixel measurement error, and more likely, 0.4 - 0.6°. For some of the features, the impact longitude can be better determined if the feature is observed at central meridian. Other estimates of the feature longitudes are available from ALPO and BAA from long term transit time measurements. Since the impact latitudes are far more southerly than the sub-earth point, the measured latitudes for the impact site may also be expected to be slighlty more southerly than the actual latitudes due to parallax by virtue of elevated impact debris above the visible cloud tops.

Preliminary results for the inferred height from measurements of the difference between the true longitude and the measured longitude and the separation from the central meridian (restricted to > 45 °) are:

Impact Feature A: 1200 km . The standard deviation is 259 km
Impact Feature H: 759 km. The standard deviation is 380 km

Other supporting evidence for the high altitude level of the impact features is provided by the appearance of the features near the terminator. The SL-9 features have been reported to be some of the darkest features ever observed on Jupiter (Chapman, C., 1994, personal communication; Rogers, 1995). These features are quite dark in appearance even when near the bright limb or the morning terminator, unlike any other features seen previously (Reese, 1994, personal communication via R. Beebe). If the features were closer in altitude to the visible cloud tops, the contrast of the features relative to the cloud features would have been reduced due to the presence of aerosols above the features.

It is known from HST images and from images obtained from La Palma (H & L impacts) that the impact process injected material as much as 3,000 km above the 1 bar level (8). Several numerical modeling of the impact process also indicate the high level of the ejected material. Recent results suggest that the impact debris ejected outward contains some Jovian material and some cometary material and that these are ejected at different velocities (9). When this debris falls back onto Jupiter, it may bounce back one or two times to fall down again. The numerical modeling of the impacts has typically been carried out only for an interval of 30 minutes, at the end of which the features are still significantly warmer than the ambient Jovian atmosphere as evidenced by earth based infrared observations (10). This suggests that convection may be present and that some impact material may indeed rise higher in the atmosphere for some time. A and H impact

sites were observed from La Palma approximately 1 hour after impact for several hours. During this period it is possible that the material may continue to rise in the Jovian atmosphere. At present we have not attempted to determine any time dependence of the altitude from the data available to us.

Finally, earth based observations of eclipses of Jovian moons indicate that considerable material believed to have been injected by the impact event was present at 160-320 km altitude between 17,000 and 23,000 km away from the impact location (11). The inferred particle size from the eclipse light curves is about 0.15 microns radius. West et al. (12) report that particles of 0.5 micron radius and smaller would remain suspended above the 100 mb level for more than 3 months in the Jovian atmosphere.

Additional measurements are expected to improve these results and extend them to other features.

References

1. The Solar Telescope of the Swedish Royal Academy of Sciences is located on La Palma, Canary Islands (28.76 deg N, 17.88 deg West, 2327 m altitude). The aperture is 50 cm and the focal length is 22.35 m @ 550 nm. The field of view is > 0.5 degrees and the image scale is 9.2 arcsec/mm.

   Scharmer, G.B., D.S. Brown, L. Pettersson, and J. Rehn, 1985. Concepts for the Swedish 50-cm vaccuum solar telescope. *Appl. Opt.*, ***24***, No. 16

2. The CCD camera is Kodak Megaplus 1.4 (1360 x 1035 pixels) with a pixel size of 6.8 micrometers producing an image scale of 0.063 arcsec/pixel. Images.

3. CCD readout noise was removed using Wiener filtering. Resulting images were then navigated using McIDAS-eXplorer software tools by finding the image center, computing the ephemeris for the observation time and using the image orientation. Image orientation was determined using Jovian moon locations in one image and then using an analytical expression for the tilt of the images with time for the telescope location. The navigated images were mapped into a rectilinear map of 0.2 degree/pixel latitude-longitude scale (700 x 640 pixels) centered at the image central meridian. The photometric function was removed in the mapping process using the Minnaert Law with the coefficients determined for each image.

   Limaye, S.S., 1994. McIDAS-eXplorer- a tool for analysis of solar system data. Applied Information Systems Newsletter, NASA, February 1994 issue.

4. Limaye, S.S., 1986. New estimates of the cloud level circulation, *Icarus*, **65,** 335-352.

5. Gierasch, P.J., B. J. Conrath, and J.A. Magalhaes, 1986. Zonal mean properties of Jupiter's upper troposphere from Voyager infrared observations, Icarus, **67**, 456-483.

6. Clarke, J.T., R. Prange, G. E. Ballester, J. Trauger, R. Evans, D. Rego, K. Stapelfeldt, W. Ip, J-C Gerard, H. Hammel, M. Ballav, L.B. Jaffel, J-L Bertaux, D. Crisp, C. Emerich, W. Harris, M. Horanyi, S. Miller, A. Storrs, and H. Weaver, 1995. HST far-ultraviolet imaging of Jupiter during the impacts of Comet Shoemaker-Levy 9, *Science*, **267**, 1302-1307.

7. Rogers, J., 1994. Jupiter's visible clouds following the comet impacts. *Bull. Amer. Astron. Soc.*, **26**, 1572-1573.

8. Hammel, H.B., R.F. Beebe, A.P. Ingersoll, G.S. Orton, J.R. Mills, A. Simon, P. Chodas, J.T. Clarke, E. DeJong, T.E. Dowling, J. Harrington, L.F. Huber, E.

Karkoschka, C.M. Santori, A. Toigo, D. Yeomans, and R.A. West, 1995. HST imaging of atmospheric phenomenon created by the impact of comet Shoemaker-Levy 9, *Science*, **267**, 1288-1296.

9. Mac Low, M.-M., K. Zahnle 1994. Explosion of Comet Shoemaker-Levy 9 on Entry into the Jovian Atmosphere. *Astrophys. J. Lett.* **434**, L33-L36.

10. Orton, G.S., et al., 1995. The NASA Infrared Telescope Facility investigation of Comet Shoemaker-Levy 9 and its collision with Jupiter: preliminary results, *Science*, **267**, 1277-1282.

11. Mallama et al., 1995. Submitted to JGR-Planets

12. West, R.A., E. Karkoschka, J. Friedson, M. Seymour, K.H. Baines, and H.B. Hammel, 1995. Impact debris particles in Jupiter's stratosphere. Science, 267, 1296-1301.

This work was supported by funds from the Space Science and Engineering Center, University of Wisconsin-Madison.

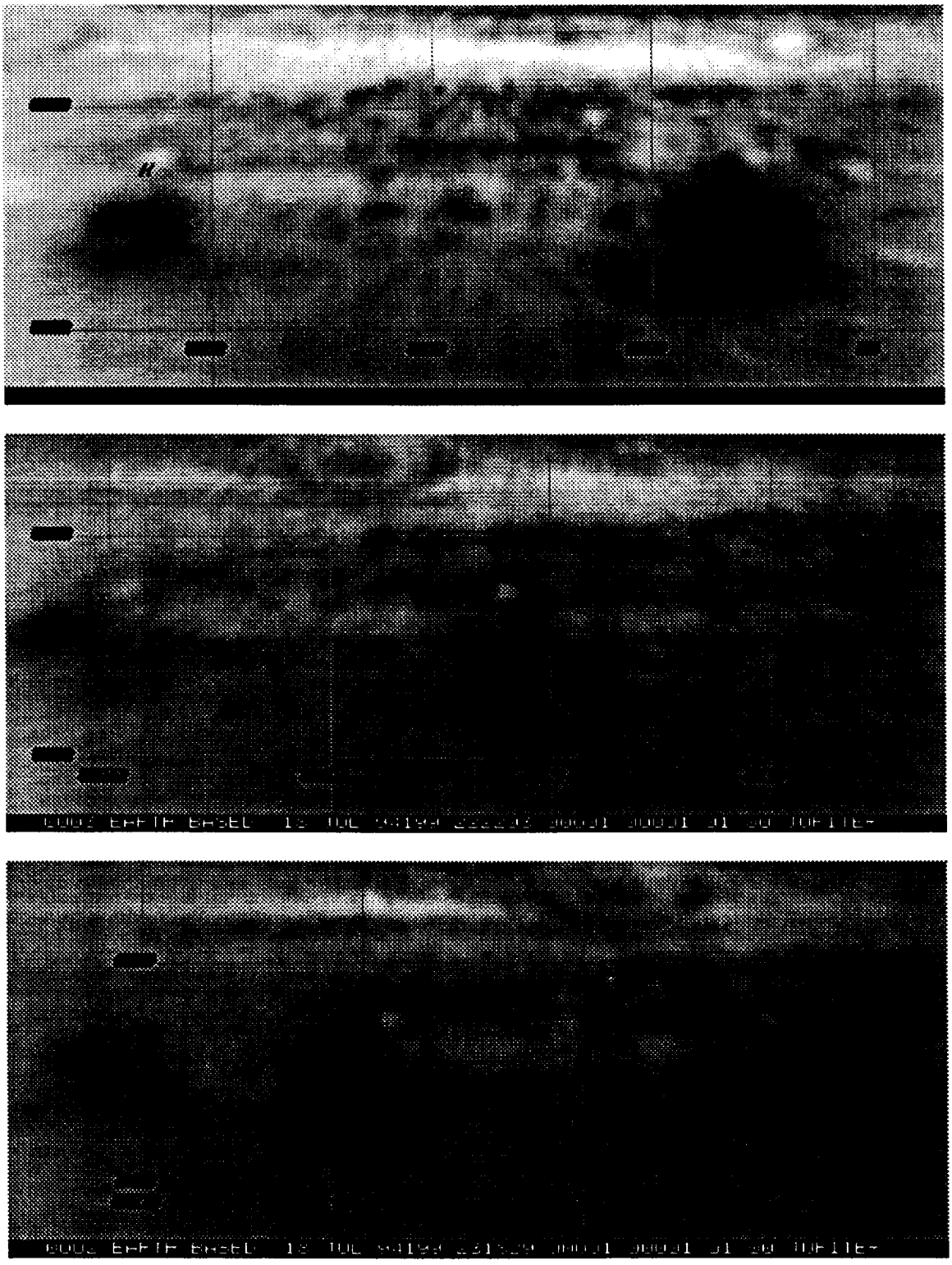

Figure 1. Apearance of H fragment impact location on Jupiter when observed far west of the central meridian (top), near the meridian (middle), and east of the central meridian (bottom). These views were created from visible band images acquired from the Swedish Solar Telescope at La Palma. The original images have been mapped into a latitude-longitude map with a 0.2 degree per pixel scale. The limb darkening has been removed using Minnaert Law. The central meridian in each image is along a vertical at the center of each image.

Figure 2. Position of H impact site measured from July 18 and 21 images.

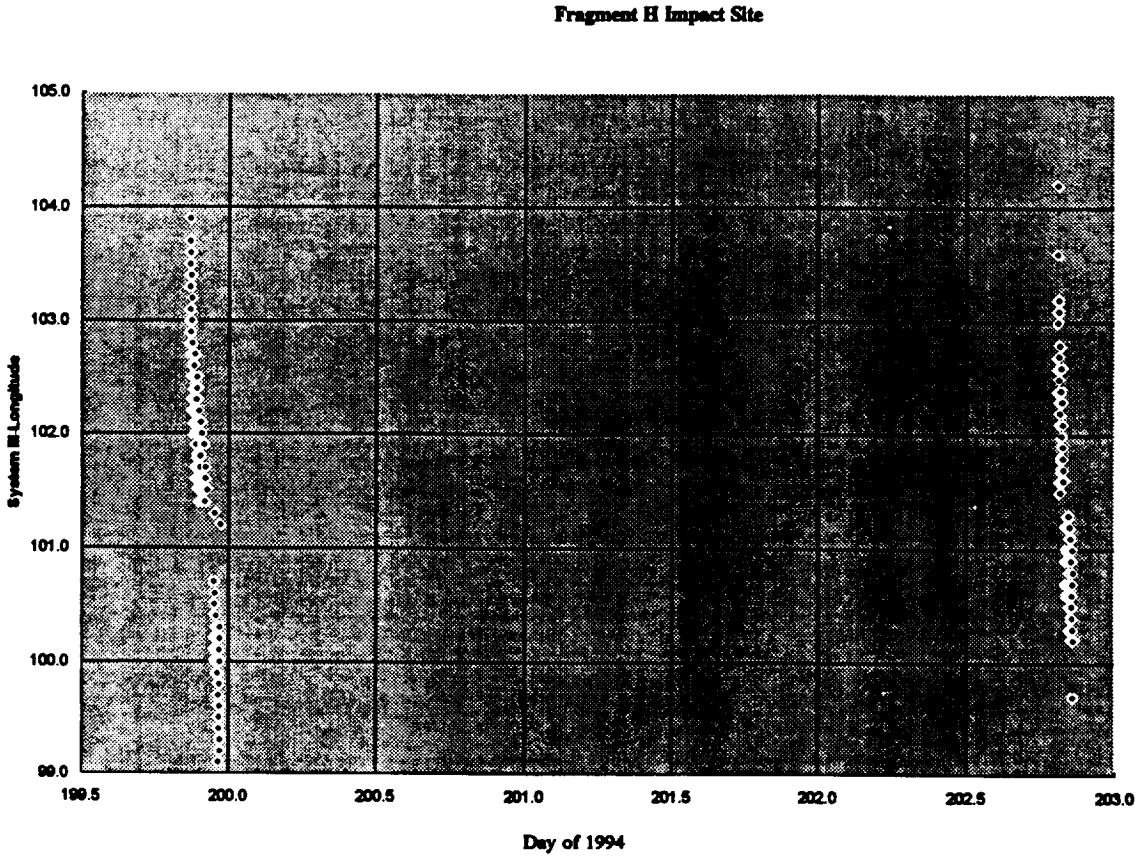

Figure 3. Variation of the H impact site brightness with age (since impact).

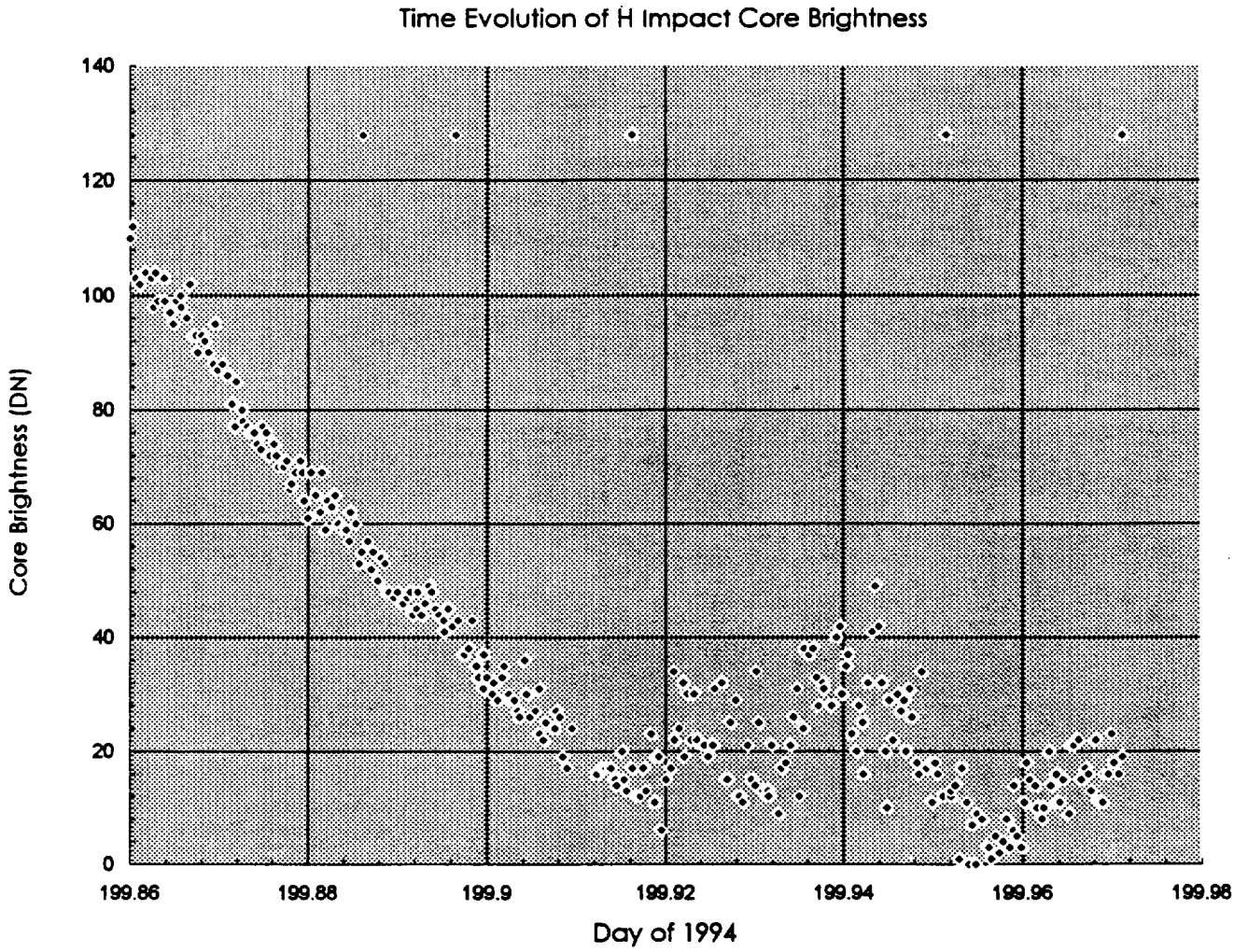

Figure 4. Impact Feature viewing geometry illustrating the parallax due to significant elevation of the feature above the visible cloud deck of Jupiter.

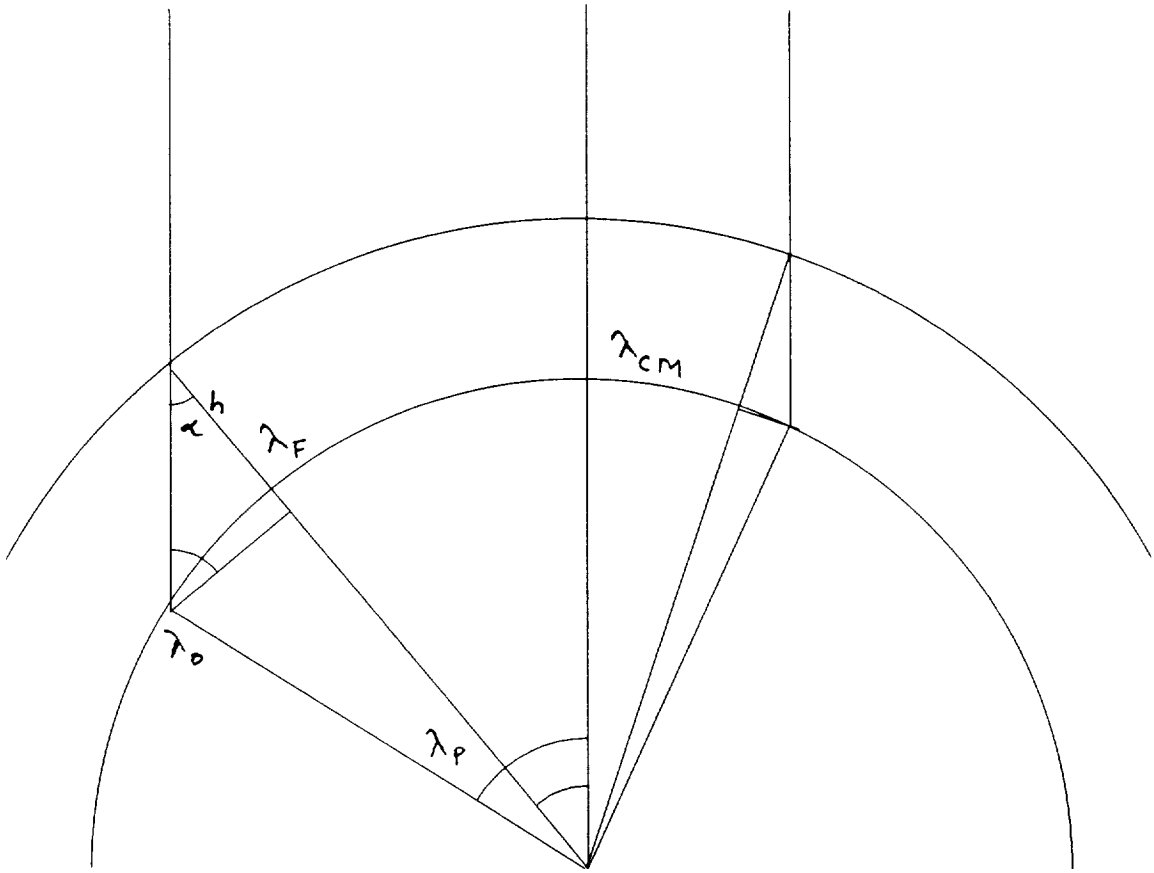

Appendix

Position Measurements for Impact Site A from the La Palma Images

Site	Day-of-1994	Age,H	Latitude	Err	SysIII Longitude	Err	Angle from Central Meridian (Deg)	Image Central Meridian Longitude	Measured Parallax Angle (Deg)	Inferred Impact Debris Altitude (KM)	Core Brightness (DN)	N
A	197.900681	1.39	-45.0	0.0	187.4	0.0	-53.9	132.4	-1.07	675.8	114	1
A	197.900681	1.39	-45.0	0.0	187.4	0.0	-53.9	132.4	-1.07	675.8	114	1
A	197.900833	1.40	-45.4	0.7	188.0	0.7	-53.8	132.5	-1.67	1050.4	115	6
A	197.900833	1.40	-45.2	0.0	188.6	0.0	-53.8	132.5	-2.30	1437.7	115	2
A	197.901382	1.41	-45.5	0.3	188.7	0.5	-53.3	133.0	-2.41	1528.3	119	5
A	197.90184	1.42	-45.0	0.2	188.3	0.2	-52.9	133.4	-2.01	1303.3	113	3
A	197.902176	1.43	-45.3	0.2	188.2	0.3	-52.6	133.7	-1.89	1239.9	111	5
A	197.902252	1.43	-45.2	0.0	188.5	0.0	-52.6	133.7	-2.23	1460.8	111	1
A	197.902817	1.44	-45.4	0.0	188.4	0.0	-52.1	134.2	-2.13	1425.2	109	1
A	197.903061	1.45	-45.3	0.0	188.1	0.0	-51.9	134.4	-1.84	1239.7	109	2
A	197.903625	1.46	-45.1	0.2	188.1	0.2	-51.4	134.9	-1.78	1224.6	110	4
A	197.903931	1.47	-45.2	0.2	188.5	0.1	-51.1	135.2	-2.16	1492.9	111	3
A	197.904251	1.48	-45.1	0.0	188.1	0.0	-50.8	135.5	-1.78	1245.0	107	2
A	197.904373	1.48	-45.3	0.0	187.9	0.0	-50.7	135.6	-1.59	1118.5	107	2
A	197.904724	1.49	-45.4	0.1	188.5	0.3	-50.4	135.9	-2.23	1578.5	110	5
A	197.905273	1.50	-45.8	0.0	188.6	0.0	-49.9	136.4	-2.26	1629.0	113	1
A	197.905548	1.51	-45.5	0.1	187.8	0.4	-49.7	136.6	-1.51	1108.9	108	3
A	197.90596	1.52	-45.1	0.0	188.3	0.0	-49.3	137.0	-1.97	1452.4	105	2
A	197.906479	1.53	-45.6	0.0	187.8	0.0	-48.9	137.4	-1.52	1145.9	106	1
A	197.90683	1.54	-45.6	0.2	187.7	0.5	-48.6	137.7	-1.36	1035.3	107	3
A	197.907028	1.55	-45.1	0.0	187.4	0.0	-48.4	137.9	-1.09	842.2	105	2
A	197.907303	1.55	-45.5	0.3	188.3	0.5	-48.2	138.1	-2.01	1545.2	108	7
A	197.907715	1.56	-44.8	0.2	187.7	0.2	-47.8	138.5	-1.40	1096.5	107	3
A	197.908112	1.57	-45.2	0.0	188.0	0.0	-47.5	138.8	-1.74	1377.8	100	1
A	197.908646	1.58	-45.4	0.0	187.9	0.0	-47.0	139.3	-1.60	1292.1	103	1
A	197.908951	1.59	-45.7	0.1	188.2	0.1	-46.7	139.6	-1.93	1566.7	105	3
A	197.909195	1.60	-45.1	0.2	187.7	0.2	-46.5	139.8	-1.37	1123.5	104	5
A	197.909607	1.61	-44.8	0.0	186.9	0.0	-46.2	140.1	-0.64	536.2	105	1
A	197.910065	1.62	-45.6	0.0	187.9	0.0	-45.8	140.5	-1.64	1383.4	104	1
A	197.910446	1.63	-45.6	0.2	187.7	0.2	-45.4	140.9	-1.38	1174.3	104	3
A	197.910461	1.63	-45.4	0.3	187.5	0.3	-45.4	140.9	-1.17	998.8	103	11
A	197.911041	1.64	-45.6	0.0	189.0	0.0	-44.9	141.4	-2.69	2311.0	102	1
A	197.911041	1.64	-45.6	0.0	189.0	0.0	-44.9	141.4	-2.69	2311.0	102	1
A	197.911041	1.64	-45.6	0.0	189.0	0.0	-44.9	141.4	-2.69	2311.0	102	1
A	197.911041	1.64	-45.6	0.0	189.0	0.0	-44.9	141.4	-2.69	2311.0	102	1
A	197.911362	1.65	-45.1	0.3	187.3	0.3	-44.6	141.7	-1.05	921.8	101	7
A	197.911591	1.66	-45.2	0.2	187.7	0.2	-44.4	141.9	-1.36	1205.6	100	3
A	197.91214	1.67	-45.1	0.3	187.6	0.3	-44.0	142.3	-1.27	1147.6	101	14
A	197.912277	1.67	-45.7	0.2	187.9	0.2	-43.8	142.5	-1.65	1484.5	100	5
A	197.912949	1.69	-45.3	0.2	187.1	0.1	-43.2	143.1	-0.75	697.3	101	4
A	197.913284	1.70	-45.2	0.2	187.6	0.1	-43.0	143.3	-1.28	1197.5	99	5
A	197.913406	1.70	-45.2	0.0	186.4	0.0	-42.9	143.4	-0.14	136.0	103	1
A	197.914017	1.71	-44.8	0.0	187.6	0.0	-42.3	144.0	-1.28	1219.0	99	1
A	197.914169	1.72	-45.6	0.1	188.2	0.1	-42.2	144.1	-1.91	1820.0	101	4
A	197.914429	1.72	-45.1	0.1	187.6	0.1	-42.0	144.3	-1.31	1263.2	97	3

Site	Day-of-1994	Age,H	Latitude	Err	SysIII Longitude	Err	Angle from Central Meridian (Deg)	Image Central Meridian Longitude	Measured Parallax Angle (Deg)	Inferred Impact Debris Altitude (KM)	Core Brightness (DN)	N
A	197.930984	2.12	-45.3	0.2	186.0	0.2	-27.6	158.7	0.25	-422.7	85	10
A	197.931625	2.14	-45.2	0.0	186.1	0.0	-27.0	159.3	0.19	-320.8	84	1
A	197.931671	2.14	-44.8	0.2	186.2	0.3	-26.9	159.4	0.15	-252.2	93	3
A	197.932129	2.15	-45.4	0.0	187.1	0.0	-26.6	159.7	-0.85	1481.9	83	1
A	197.932495	2.16	-45.1	0.2	186.7	0.2	-26.2	160.1	-0.45	798.2	85	5
A	197.93306	2.17	-45.2	0.0	186.8	0.0	-25.7	160.6	-0.46	841.2	78	1
A	197.933289	2.18	-45.3	0.1	186.4	0.1	-25.5	160.8	-0.12	221.4	83	3
A	197.933594	2.18	-44.8	0.0	186.4	0.0	-25.3	161.0	-0.12	215.4	79	1
A	197.933929	2.19	-45.4	0.0	187.1	0.0	-25.0	161.3	-0.81	1518.1	84	1
A	197.934509	2.21	-45.2	0.0	186.4	0.0	-24.5	161.8	-0.11	215.7	85	1
A	197.934616	2.21	-45.5	0.1	186.8	0.1	-24.4	161.9	-0.48	926.8	76	3
A	197.935226	2.22	-45.0	0.2	186.4	0.1	-23.9	162.4	-0.14	271.7	81	3
A	197.935349	2.23	-44.9	0.0	186.5	0.0	-23.8	162.5	-0.25	494.1	80	2
A	197.935852	2.24	-45.7	0.1	186.9	0.1	-23.3	163.0	-0.56	1133.5	92	3
A	197.935989	2.24	-45.3	0.2	186.6	0.2	-23.2	163.1	-0.27	549.6	85	9
A	197.936584	2.26	-44.9	0.2	186.5	0.2	-22.7	163.6	-0.18	369.5	85	4
A	197.936951	2.26	-45.3	0.0	186.4	0.0	-22.4	163.9	-0.14	294.3	78	2
A	197.937363	2.27	-45.3	0.0	186.6	0.0	-22.0	164.3	-0.30	653.1	81	2
A	197.9375	2.28	-44.5	0.0	186.2	0.0	-21.9	164.4	0.08	-170.5	75	2
A	197.93811	2.29	-44.9	0.0	186.6	0.0	-21.3	165.0	-0.26	574.4	82	2
A	197.938156	2.29	-45.5	0.2	186.7	0.2	-21.3	165.0	-0.36	815.2	81	6
A	197.93869	2.31	-44.8	0.0	185.9	0.0	-20.8	165.5	0.44	-1015.8	74	1
A	197.939072	2.31	-45.1	0.2	186.0	0.2	-20.5	165.8	0.31	-723.4	77	10
A	197.939499	2.33	-45.6	0.0	187.0	0.0	-20.1	166.2	-0.66	1588.3	83	1
A	197.939743	2.33	-45.4	0.2	186.8	0.1	-19.9	166.4	-0.48	1153.3	90	3
A	197.940109	2.34	-45.2	0.0	186.6	0.0	-19.6	166.7	-0.29	711.2	90	2
A	197.940567	2.35	-45.3	0.3	186.8	0.1	-19.2	167.1	-0.49	1237.5	88	4
A	197.940842	2.36	-45.3	0.1	186.5	0.2	-19.0	167.3	-0.23	597.1	81	3
A	197.941055	2.36	-45.0	0.2	186.1	0.2	-18.8	167.5	0.18	-477.5	80	5
A	197.941452	2.37	-45.2	0.1	186.3	0.1	-18.4	167.9	0.00	-5.3	74	5
A	197.941879	2.38	-44.8	0.0	186.2	0.0	-18.1	168.2	0.07	-185.6	79	1
A	197.942429	2.40	-45.4	0.2	186.0	0.1	-17.6	168.7	0.25	-700.1	84	3
A	197.942627	2.40	-45.2	0.1	186.7	0.2	-17.4	168.9	-0.42	1169.1	89	6
A	197.942917	2.41	-45.6	0.0	186.5	0.0	-17.2	169.1	-0.24	673.0	77	1
A	197.94339	2.42	-45.3	0.1	186.2	0.2	-16.8	169.6	0.15	-437.5	76	3
A	197.943558	2.42	-45.2	0.2	186.1	0.1	-16.6	169.7	0.17	-494.5	78	5
A	197.943939	2.43	-45.6	0.0	186.9	0.0	-16.3	170.0	-0.62	1872.7	82	2
A	197.94458	2.45	-45.8	0.1	186.5	0.3	-15.7	170.6	-0.25	773.2	84	5
A	197.944763	2.45	-45.5	0.0	186.7	0.0	-15.6	170.7	-0.45	1414.4	88	2
A	197.945282	2.46	-45.1	0.1	185.9	0.2	-15.1	171.2	0.45	-1455.7	78	4
A	197.945633	2.47	-45.5	0.1	186.5	0.2	-14.8	171.5	-0.21	680.9	75	3
A	197.945786	2.48	-45.0	0.2	185.8	0.1	-14.7	171.6	0.46	-1557.8	79	4
A	197.946152	2.48	-45.0	0.2	186.4	0.1	-14.3	172.0	-0.10	339.8	80	5
A	197.946579	2.50	-45.1	0.2	185.8	0.2	-14.0	172.3	0.51	-1808.1	75	3
A	197.947006	2.51	-44.8	0.1	186.3	0.2	-13.6	172.7	0.05	-166.8	73	5

Site	Day-of-1994	Age,H	Latitude	Err	SysIII Longitude	Err	Angle from Central Meridian (Deg)	Image Central Meridian Longitude	Measured Parallax Angle (Deg)	Inferred Impact Debris Altitude (KM)	Core Brightness (DN)	N
A	197.963577	2.90	-45.0	0.0	185.8	0.0	0.8	187.1	0.48	29236.8	64	2
A	197.963638	2.90	-45.0	0.0	185.4	0.0	0.9	187.2	0.92	52206.8	68	1
A	197.963974	2.91	-45.2	0.2	185.6	0.1	1.2	187.5	0.72	31015.9	73	4
A	197.96463	2.93	-45.5	0.2	185.1	0.1	1.7	188.0	1.16	33547.1	69	4
A	197.964981	2.94	-45.2	0.0	185.6	0.2	2.0	188.3	0.66	16192.5	63	4
A	197.965088	2.94	-45.2	0.0	186.0	0.0	2.1	188.4	0.27	6317.0	64	1
A	197.965424	2.95	-45.4	0.0	185.6	0.0	2.4	188.7	0.68	14010.8	73	2
A	197.965942	2.96	-45.4	0.0	185.2	0.0	2.9	189.2	1.11	19333.9	62	1
A	197.9664	2.97	-45.6	0.0	185.3	0.2	3.3	189.6	1.02	15591.1	70	4
A	197.966766	2.98	-45.6	0.0	185.3	0.0	3.6	189.9	1.01	14065.5	74	1
A	197.966843	2.98	-45.3	0.2	185.5	0.2	3.7	190.0	0.84	11451.4	68	12
A	197.96727	2.99	-46.3	0.2	185.4	0.1	4.0	190.3	0.90	11154.5	82	3
A	197.967651	3.00	-45.1	0.1	185.2	0.3	4.4	190.7	1.06	12216.3	71	6
A	197.967957	3.01	-45.0	0.0	185.5	0.0	4.6	190.9	0.76	8200.8	67	1
A	197.968338	3.02	-45.8	0.2	185.2	0.2	5.0	191.3	1.08	10886.3	69	11
A	197.968933	3.03	-45.3	0.1	185.4	0.1	5.5	191.8	0.91	8334.4	72	4
A	197.969162	3.04	-45.5	0.0	185.1	0.0	5.7	192.0	1.22	10763.2	75	2
A	197.969543	3.05	-46.2	0.0	185.3	0.0	6.0	192.3	0.98	8138.1	71	1
A	197.969955	3.06	-45.2	0.2	185.2	0.1	6.4	192.7	1.13	8835.7	67	4
A	197.970154	3.06	-45.3	0.1	184.6	0.2	6.5	192.8	1.74	13289.9	63	7
A	197.970764	3.08	-45.4	0.0	184.7	0.2	7.1	193.4	1.62	11434.0	64	4
A	197.970795	3.08	-45.6	0.0	185.2	0.0	7.1	193.4	1.09	7659.4	67	2
A	197.971252	3.09	-45.6	0.3	186.1	0.3	7.5	193.8	0.23	1541.3	72	3
A	197.971558	3.09	-45.7	0.2	185.1	0.2	7.8	194.1	1.19	7622.7	73	4
A	197.972137	3.11	-46.0	0.2	185.2	0.2	8.3	194.6	1.06	6396.9	74	10
A	197.972321	3.11	-45.4	0.0	185.1	0.0	8.4	194.7	1.17	6924.1	69	1
A	197.972656	3.12	-44.8	0.0	184.6	0.0	8.7	195.0	1.67	9508.0	66	1
A	197.973267	3.14	-45.4	0.0	185.4	0.0	9.3	195.6	0.94	5076.5	68	1
A	197.973358	3.14	-45.2	0.1	184.6	0.2	9.3	195.6	1.66	8860.4	71	4
A	197.974014	3.15	-46.0	0.2	184.8	0.2	9.9	196.2	1.46	7336.1	84	8
A	197.974045	3.15	-46.1	0.1	185.0	0.3	9.9	196.2	1.27	6347.9	83	7
A	197.974396	3.16	-45.9	0.2	185.2	0.2	10.2	196.5	1.06	5124.6	82	4
A	197.975052	3.18	-46.3	0.1	184.8	0.2	10.8	197.1	1.49	6846.3	80	6
A	197.975327	3.19	-45.6	0.3	185.2	0.3	11.0	197.3	1.08	4826.8	79	8
A	197.975754	3.20	-45.4	0.0	184.7	0.0	11.4	197.7	1.58	6834.6	72	1
A	197.976074	3.20	-45.4	0.0	184.6	0.0	11.7	198.0	1.70	7161.7	67	1
A	197.976395	3.21	-44.8	0.2	185.0	0.1	12.0	198.3	1.32	5463.9	59	4
A	197.976776	3.22	-44.9	0.0	184.9	0.0	12.3	198.6	1.39	5579.3	66	2
A	197.977539	3.24	-41.4	0.0	185.5	0.0	13.0	199.3	0.83	3141.1	108	1
A	197.977905	3.25	-45.8	0.2	184.6	0.3	13.3	199.6	1.68	6199.6	70	7
A	197.978149	3.25	-45.4	0.0	185.0	0.0	13.5	199.8	1.29	4706.8	79	2
A	197.978653	3.26	-46.4	0.0	184.7	0.0	14.0	200.3	1.65	5803.8	75	1
A	197.978989	3.27	-44.6	0.2	185.3	0.2	14.2	200.5	0.96	3301.6	68	5
A	197.979309	3.28	-45.2	0.0	185.2	0.0	14.5	200.8	1.08	3668.6	71	1
A	197.979614	3.29	-45.3	0.0	184.6	0.0	14.8	201.1	1.71	5671.8	72	2

Site	Day-of-1994	Age,H	Latitude	Err	SysIII Longitude	Err	Angle from Central Meridian (Deg)	Image Central Meridian Longitude	Measured Parallax Angle (Deg)	Inferred Impact Debris Altitude (KM)	Core Brightness (DN)	N
A	197.997299	3.71	-46.5	0.0	182.8	0.0	30.2	216.5	3.52	5208.8	75	2
A	197.997604	3.72	-46.7	0.1	183.3	0.1	30.4	216.7	2.95	4343.4	77	3
A	197.998413	3.74	-45.8	0.0	184.1	0.0	31.1	217.4	2.25	3227.3	75	1
A	197.998749	3.75	-46.0	0.4	183.4	0.4	31.4	217.7	2.86	4038.0	81	4
A	197.998962	3.75	-45.5	0.1	183.3	0.2	31.6	217.9	3.05	4266.3	70	5
A	197.999329	3.76	-46.3	0.4	183.2	0.3	31.9	218.2	3.05	4224.8	79	9
A	197.999725	3.77	-46.1	0.0	183.7	0.0	32.3	218.6	2.61	3572.8	67	2
A	198.000168	3.78	-45.6	0.0	183.9	0.0	32.7	219.0	2.42	3263.4	70	2
A	198.000595	3.79	-46.0	0.0	183.4	0.0	33.1	219.4	2.95	3904.8	71	1
A	198.000778	3.80	-46.5	0.3	183.0	0.3	33.2	219.5	3.27	4297.4	79	11
A	198.001114	3.80	-46.0	0.0	183.5	0.0	33.5	219.8	2.80	3653.9	74	2
A	198.001419	3.81	-46.2	0.1	183.4	0.2	33.8	220.1	2.88	3714.7	75	4
A	198.002045	3.83	-46.4	0.0	183.9	0.0	34.3	220.6	2.39	3023.5	69	2
A	198.00206	3.83	-46.4	0.0	183.7	0.0	34.3	220.6	2.58	3259.2	72	2
A	198.002472	3.84	-46.2	0.0	182.8	0.2	34.7	221.0	3.52	4372.5	73	3
A	198.002945	3.85	-46.0	0.0	183.4	0.0	35.1	221.4	2.91	3568.7	81	1
A	198.003815	3.87	-46.6	0.3	183.3	0.3	35.9	222.2	2.98	3547.2	75	6
A	198.004532	3.89	-46.2	0.2	183.7	0.3	36.5	222.8	2.61	3045.7	76	5
A	198.004852	3.89	-45.6	0.0	183.5	0.0	36.8	223.1	2.85	3283.4	66	1
A	198.005173	3.90	-46.0	0.3	183.9	0.4	37.0	223.3	2.37	2708.4	70	4
A	198.005569	3.91	-46.8	0.1	183.2	0.3	37.4	223.7	3.12	3511.3	78	6
A	198.005981	3.92	-44.8	0.0	182.8	0.0	37.7	224.0	3.46	3830.3	80	1
A	198.006271	3.93	-45.7	0.5	183.1	0.3	38.0	224.3	3.21	3525.0	75	4
A	198.006409	3.93	-47.2	0.0	182.6	0.0	38.1	224.4	3.69	4019.0	69	1
A	198.006805	3.94	-46.1	0.1	182.6	0.1	38.5	224.8	3.74	4028.2	68	4
A	198.00737	3.95	-46.5	0.0	183.0	0.0	38.9	225.2	3.25	3446.9	67	2
A	198.007599	3.96	-46.6	0.0	182.5	0.0	39.1	225.4	3.75	3931.8	69	2
A	198.007843	3.97	-45.4	0.0	183.4	0.0	42.5	228.8	2.90	2716.9	74	1
A	198.008972	3.99	-45.7	0.0	182.4	0.0	40.3	226.6	3.86	3872.8	73	2
A	198.010559	4.03	-45.7	0.4	182.5	0.5	41.7	228.0	3.78	3609.7	71	4
A	198.010834	4.04	-46.7	0.0	182.6	0.0	42.0	228.3	3.74	3539.7	78	2
A	198.013107	4.09	-47.0	0.0	182.8	0.0	43.9	230.2	3.45	3051.6	72	1
A	198.015106	4.14	-46.1	0.1	183.8	0.2	45.7	232.0	2.52	2111.2	71	3
A	198.01564	4.15	-45.4	0.0	184.0	0.0	46.1	232.4	2.26	1863.8	71	1
A	198.015869	4.16	-50.2	0.0	183.0	0.0	46.3	232.6	3.26	2643.8	81	1
A	198.016693	4.18	-46.4	0.2	182.8	0.2	47.1	233.4	3.47	2743.3	75	3
A	198.017044	4.19	-45.8	0.0	182.7	0.0	47.4	233.7	3.64	2836.5	73	1
A	198.017303	4.19	-45.0	0.4	185.5	0.3	47.6	233.9	0.84	668.2	68	6
A	198.017838	4.21	-47.0	0.0	183.2	0.0	48.1	234.4	3.14	2401.8	82	1
A	198.018097	4.21	-45.5	0.1	183.5	0.1	48.3	234.6	2.84	2162.0	81	3

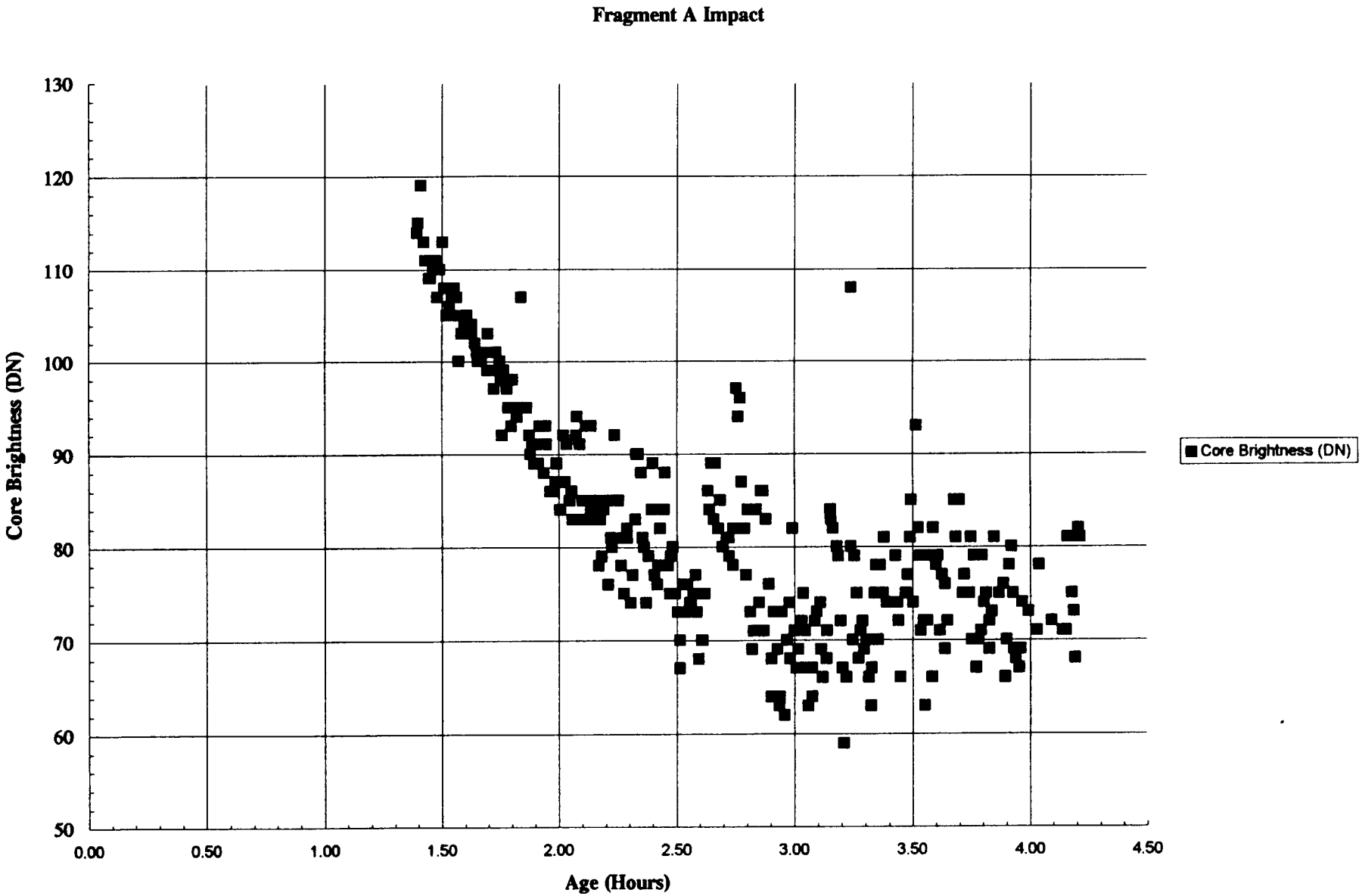
Fragment A Impact
Core Brightness (DN)
130
120
110
100
90
80
70
60
50
0.00
0.50
1.00
1.50
2.00
2.50
3.00
3.50
4.00
4.50
Age (Hours)
Core Brightness (DN)

ADATA Chart 6

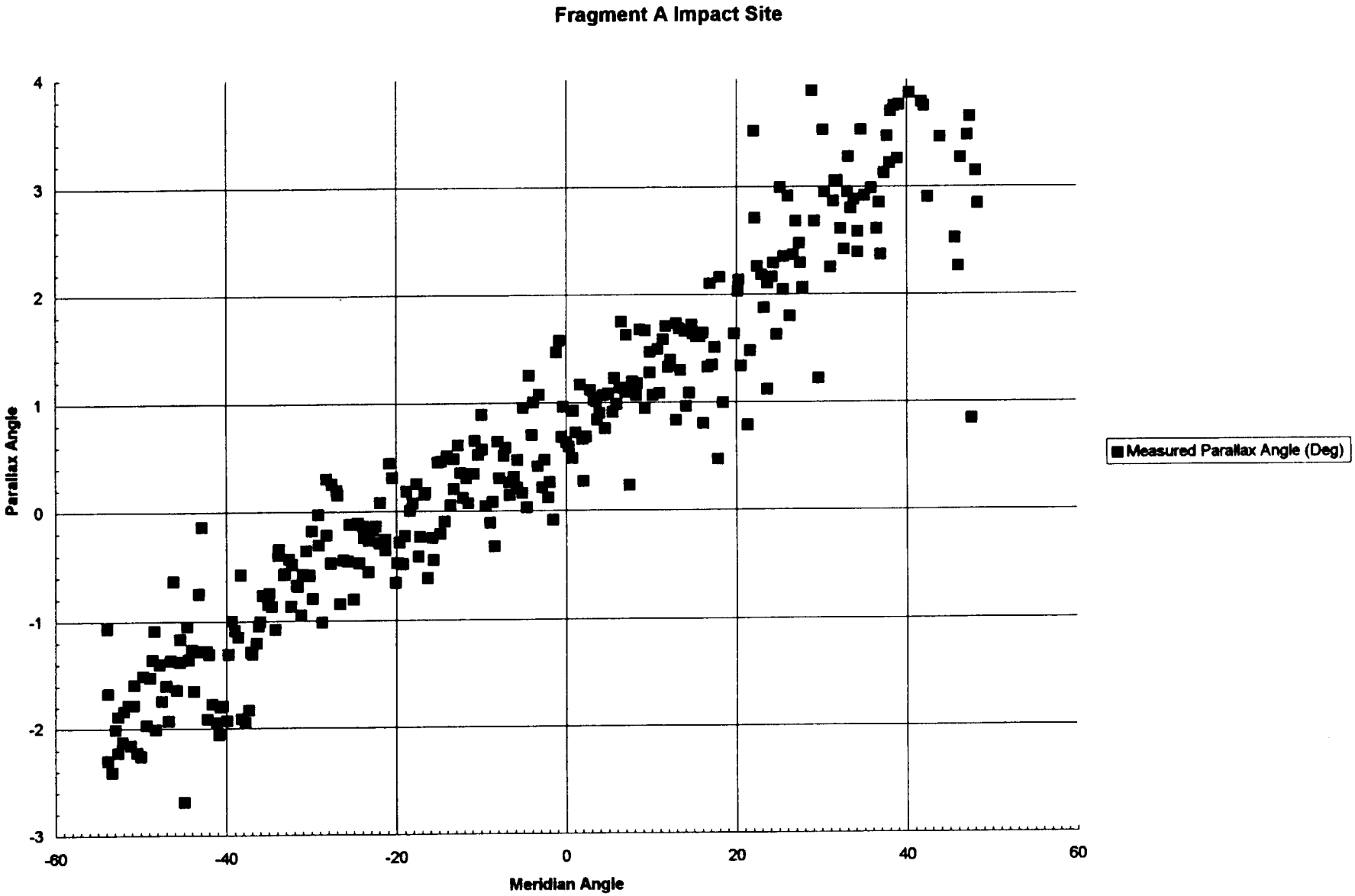

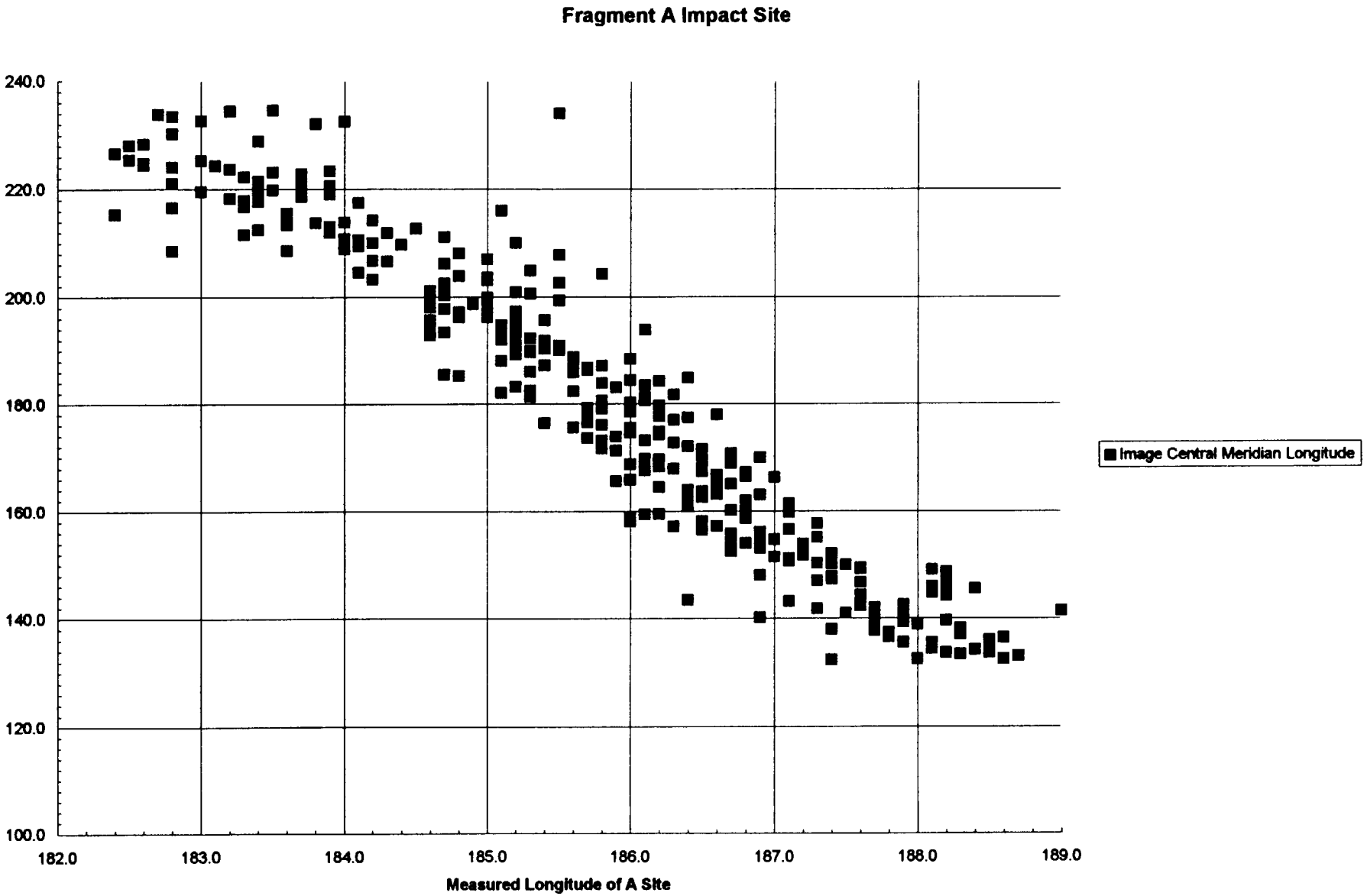
Fragment A Impact Site
240.0
220.0
200.0
180.0
160.0
140.0
120.0
100.0
182.0
183.0
184.0
185.0
186.0
187.0
188.0
189.0
Measured Longitude of A Site
Image Central Meridian Longitude

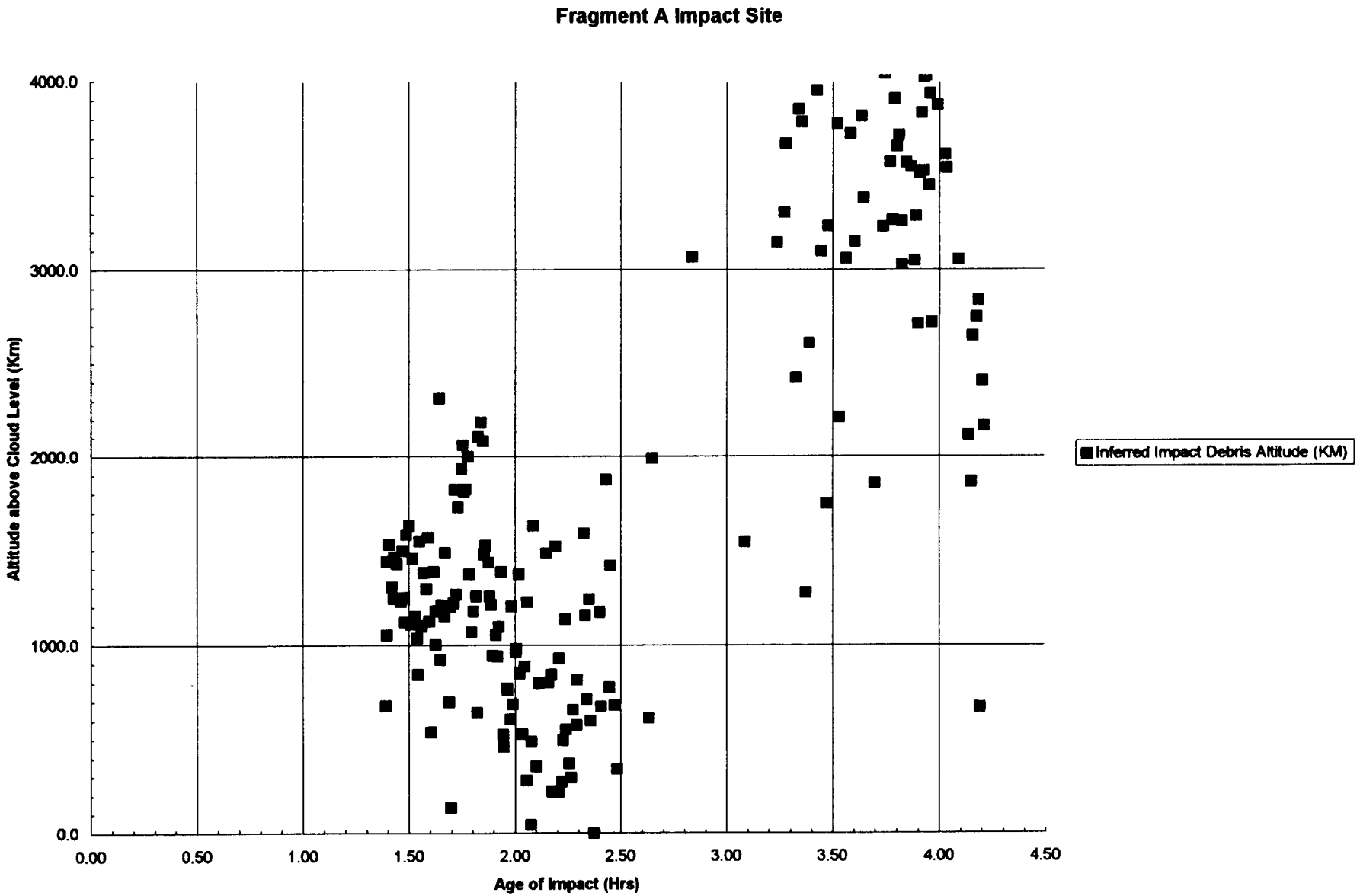
Fragment A Impact Site
Altitude above Cloud Level (Km)
4000.0
3000.0
2000.0
1000.0
0.0
0.00
0.50
1.00
1.50
2.00
2.50
3.00
3.50
4.00
4.50
Age of Impact (Hrs)
Inferred Impact Debris Altitude (KM)

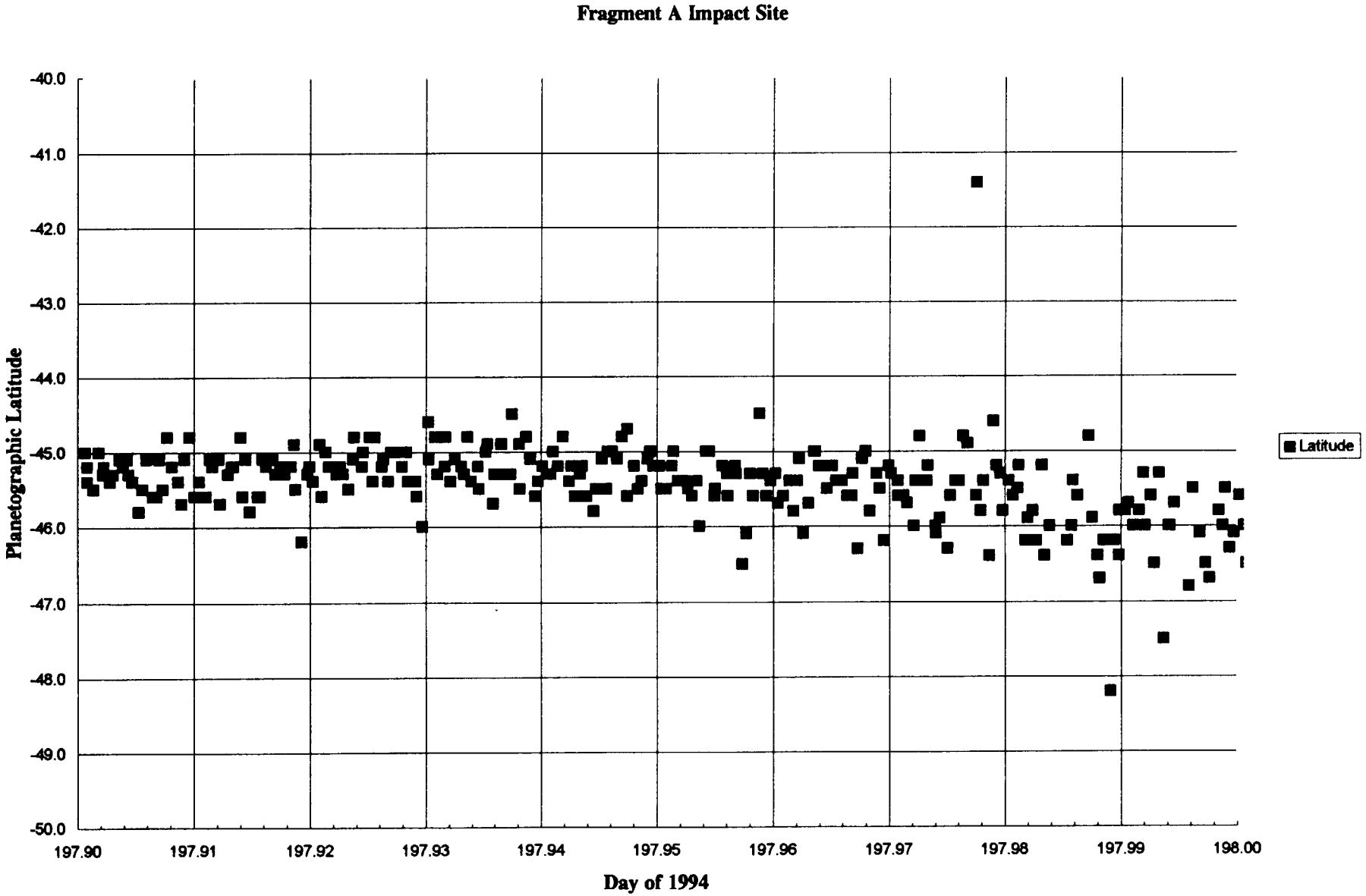
Fragment A Impact Site
Planetographic Latitude
-40.0
-41.0
-42.0
-43.0
-44.0
-45.0
-46.0
-47.0
-48.0
-49.0
-50.0
197.90
197.91
197.92
197.93
197.94
197.95
197.96
197.97
197.98
197.99
198.00
Day of 1994
Latitude

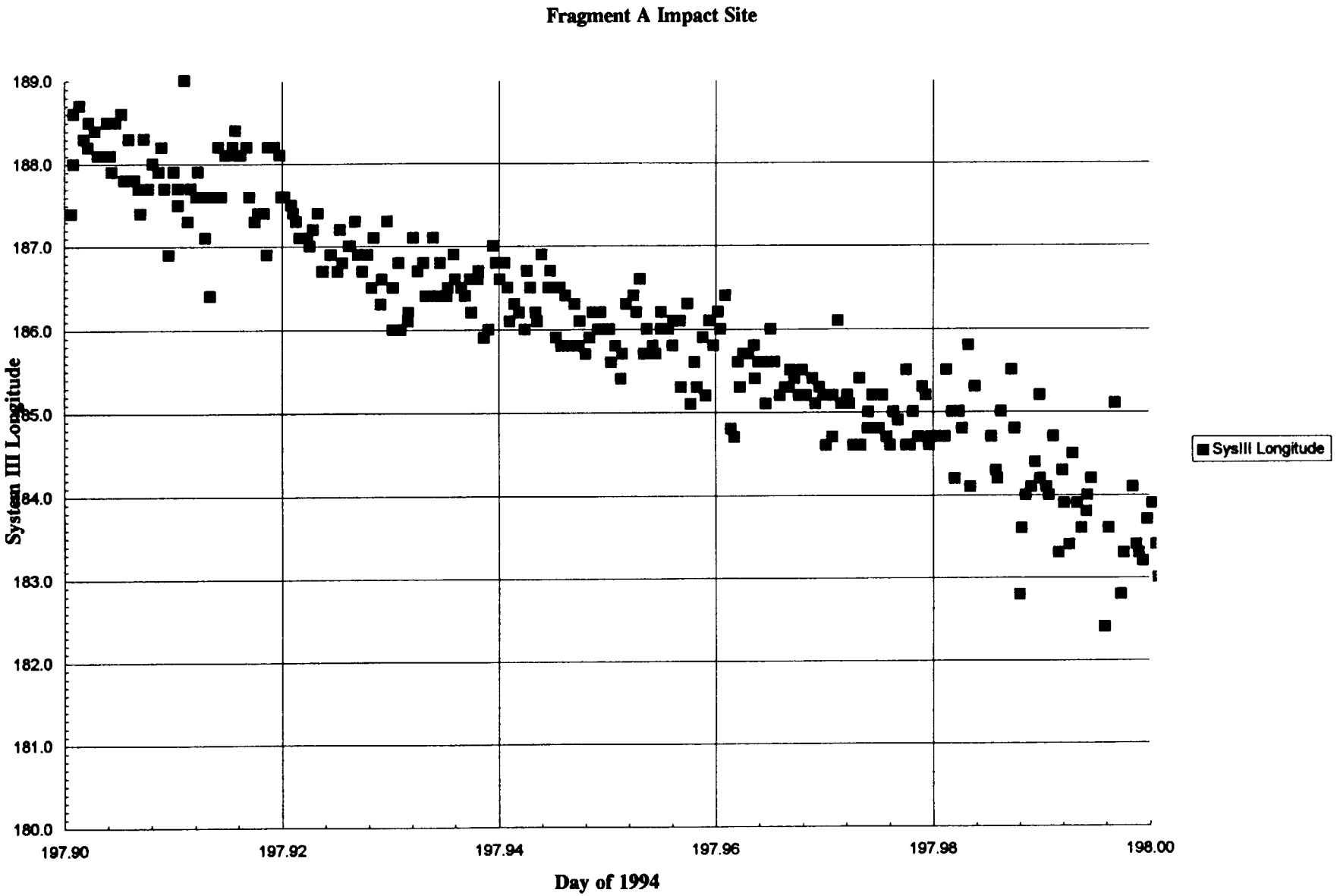
Fragment A Impact Site
189.0
188.0
187.0
186.0
185.0
184.0
183.0
182.0
181.0
180.0
System III Longitude
197.90
197.92
197.94
197.96
197.98
198.00
Day of 1994
SysIII Longitude

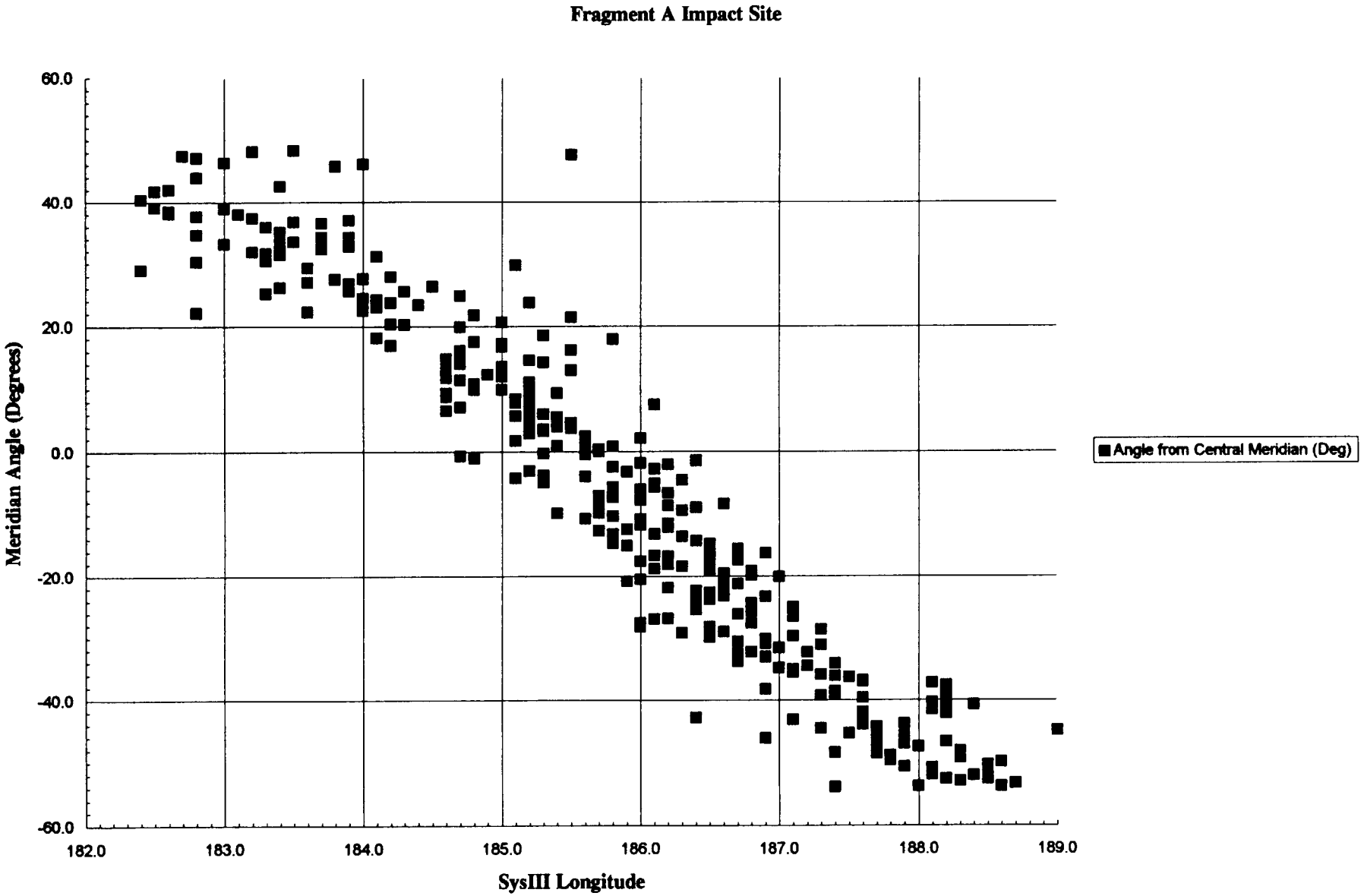
Fragment A Impact Site
60.0
40.0
20.0
0.0
-20.0
-40.0
-60.0
Meridian Angle (Degrees)
182.0
183.0
184.0
185.0
186.0
187.0
188.0
189.0
SysIII Longitude
Angle from Central Meridian (Deg)

ADATA Chart 12